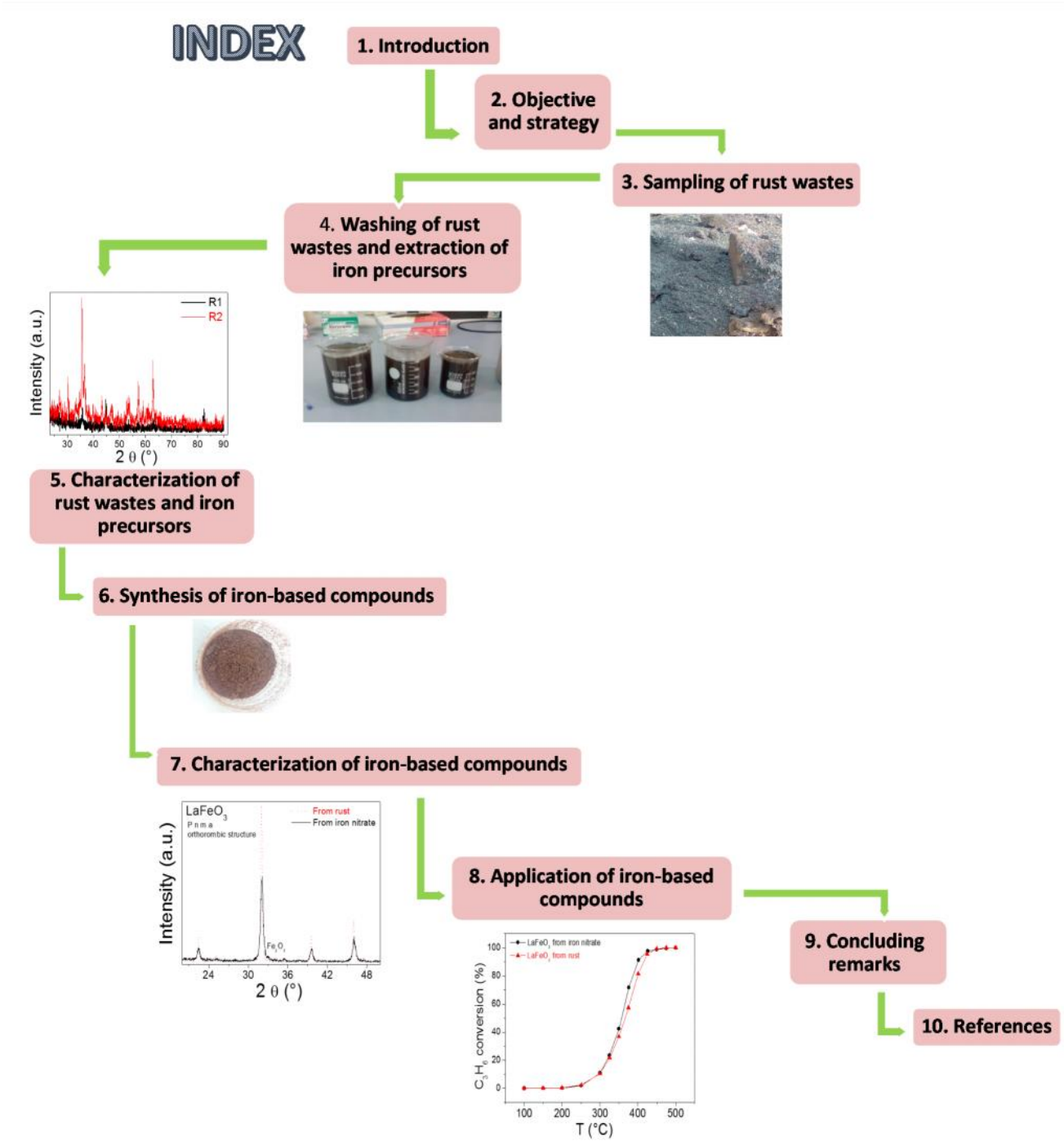

IRON-BASED PEROVSKITE-TYPE CATALYSTS FROM RUST:

A COOPERATION BETWEEN ITALY AND INDIA

by **Dr.(Mrs.) Manisha P.Joshi** (Italian coordinator: Dr. Francesca Deganello)

under the framework of **PROGRAMMA DI RICERCA STM 2016** at Istituto per lo Studio dei Materiali Nanostrutturati– Consiglio Nazionale delle Ricerche (ISMN-CNR), Palermo, Italy, from 14th November 2016 to 25th November 2016.

IRON-BASED PEROVSKITE-TYPE CATALYSTS FROM RUST:

A COOPERATION BETWEEN ITALY AND INDIA

1. INTRODUCTION

Iron-based perovskite-type catalysts are an important class of materials with multifunctional properties for applications in catalysis, solid oxide fuel cells and magnetic devices [1, 2]. The presence of iron at B-site - the “catalytic” site of the perovskite structure - ensures very good reactivity toward oxygen and oxygenated compounds [1, 2].

On the other hand, the same reactivity of iron is responsible of the rusting of iron-containing objects. In facts, iron exposed to moist air or oxygenated water is corroded, leaving a red encrustation of iron oxide on the surface, which is called rust and is mainly composed by hydrated Fe_2O_3 [3]. Progressive rusting is a major source of failure of unprotected structural materials. It is aggravated by bad design, which leaves moisture traps in the structure. Rust may pit small holes in a surface, or uniformly progress over its area. It may attack joints and crevices. (Fig. 1).

Fig. 1 Corroding iron machinery at the abandoned White Island Sulphur mine [4].

Despite their universal vulnerability to penetration, iron and steel materials are insufficiently protected, both in manufacture and in maintenance. A corrosive environment of iron or steel only requires the presence of water together with either a dissolved acid gas or oxygen, or in some cases just dissolved salts (eg brine). The importance of rust is particularly evident in the automobile industry In the UK it has been estimated that automotive rust costs some £260

RUST WASTES ARE USED AS IRON PRECURSORS FOR THE PRODUCTION OF IRON-BASED PEROVSKITES

The preferred iron precursor for the synthesis of Lanthanum Ferrite is usually Iron nitrate. The cost of iron nitrate (Sigma – Aldrich) for the synthesis of 2 grams of powder is approximately 20 Euroes. Using rust as a source of iron does not cost anything!

million per year, decreasing the value of each automobile by £1 every week. In countries exposed to ice and snow on the roads, the use of salt to clear it accelerates rusting. In the UK, where the use of salt in this way is estimated to cause 50% of rusting, it therefore costs £130 million per year. In the USA, repairs and replacements due to corrosion and rust damage may be worth nearly 5% of the gross national product. High humidity countries or locations experience the worst rusting: Suriname, Abu Dhabi and Indonesia top one list of rust-prone climates. In 1990 it was reported that the 1,300 kilometre trans-Alaska pipeline (designed to be rustproof for 30 to 40 years) was seriously corroding because of failure to corrode it adequately. Repairs were expected to cost from $600 to $1,500 million [5]. The serious consequences of the rusting of iron have become a problem of worldwide significance. In addition to our everyday encounters with this form of degradation, rusting causes plant shutdowns, waste of valuable resources, loss or contamination of product, reduction in efficiency, costly maintenance, and expensive overdesign.

In industries, before galvanizing of the iron material its surface is scrapped to remove rust from its surface. This rust must be eliminated and is usually sold as scrap at very negligible rate. In this context, a more convenient way to use the industrial iron wastes would be desirable and some possible solution have been already proposed in the recent literature. Some of the proposed solutions dealt specifically with scrap-derived iron and rust wastes [6-10]. Other valuable solutions - which in principle might also be extended and applied to rust wastes – concerned the reutilization of different industrial iron-rich wastes like waste ferrous sulfate [11], iron-removal sludge [12] and oily cold rolling mill sludge [13] and dried steel wiredrawing sludge [14].

Iron-perovskites are usually prepared from commercial iron nitrates or iron chlorides precursors [15]. Among the others, solution combustion synthesis [16, 17] is an easy and convenient method for the preparation of iron-perovskites [18]. In this attractive technique, based on the principles of the propellant chemistry [19], a thermally induced redox reaction takes place between an oxidant and a fuel. Several variants of solution combustion synthesis exist, which have been widely described in the literature, demonstrating the large versatility of this powerful technique [16, 17, 20-24]. By combustion-based methods, it is possible to produce monophasic nanopowders with homogeneous microstructure, at lower temperatures or shorter reaction times, if compared with other conventional methods like solid-state synthesis [25, 26] or nitrate method [27, 28]. Moreover, the possibility to use waste-derived precursors adds a further advantage to this powerful methodology [29].

2. OBJECTIVE AND STRATEGY

Objective of this work is to replace the commercial iron nitrate with rust as a source of iron for the synthesis of a $LaFeO_3$ powder by solution combustion synthesis (SCS).

The main advantage of using SCS is that solid precursors can also be used, without compromising to much the chemical and microstructural homogeneity of the obtained powder [30, 31].

A detailed comparison with a standard powder obtained by SCS starting from a conventional iron precursor (commercial iron nitrate) is also performed.

An accurate characterization of the rust wastes as well as of the perovskite powders is mandatory in order to understand drawbacks and peculiarities of this new approach. The characterization techniques used in this work are:

- Powder X-ray diffraction (XRD) coupled with Rietveld Refinement analysis

- Temperature programmed reduction (TPR)
- X-ray photoelectron spectroscopy (XPS)
- Fourier Transform analysis (FT-IR)

The choice of $LaFeO_3$ as iron-based compound is twofold. First, the simplicity of this chemical composition, with only one metal beside Fe, limits any possible multiphase segregation and avoids useless complexity to the results interpretation. Second, by "testing" the possibility of using rust wastes as iron precursors directly on a perovskite compound - instead of on a simple iron-based oxide - enlarges the applicability of the synthesis to a wider class of iron-based compounds and to a variety of technological uses.

The performance of this ecofriendly material is evaluated by testing the activity and selectivity in the propylene oxidation, in order to use it for the benefit of the environment. Although the most active perovskite-type formulations of oxidation catalysts are multielemental, $LaFeO_3$ is often taken as a model of iron-based perovskite [29, 32, 33]. Moreover, it shows itself a discrete activity as sensor [34], photocatalyst [29, 35] and oxidation catalyst [36-40].

3. SAMPLING OF RUST

Rust wastes were collected in powdered form from the transmission line tower manufacturing unit of an Electricity transmission tower manufacturing industry near Nagpur, INDIA (**Fig.2**).

Fig 2. : Pictures showing Collection of rust wastes from Electricity transmission tower manufacturing industry near Nagpur (INDIA)

THREE TYPES OF IRON WASTES HAVE BEEN EXTRACTED FROM RUST

The scrap treatment caused a large amount of metallic iron to be present in the "rust" wastes. We separated three iron-wastes, differing for the metallic iron/iron oxides content.

R1 is simply the washed iron waste; R2 and R3 were extracted from the powdered suspension and from the sediment during washing, respectively

4. WASHING OF RUST AND EXTRACTION OF IRON PRECURSORS

The as-received rust was washed in a stainless steel beaker with distilled water at about 90°C for 1h. Sometimes it was stirred manually by using a big stainless steel spatula. Then the water was taken out of the beaker and replaced with clean cold water. The washed rust was dried overnight in the oven at 80°C. It was magnetic and brown and it was called R1. In Fig.3, the magnetic nature of R1 is shown.

Fig 3 : Magnetic nature of rust-derived iron precursors

The washing water was not transparent, but gray-black with some brownish powdered suspension as in Fig 4. Therefore, the suspension was separated and the sediment allowed to deposit. Then most of the water was taken out and the powder was dried overnight in the oven at 80 °C. The powder was reddish and magnetic and it was called R2.

Fig 4. Washing waters after the washing treatment (side and top view).

We also washed a small portion of the rust many times until the washing water was clear. This rust was brownish, it was magnetic and it was called R3.

5. CHARACTERIZATION OF IRON PRECURSORS

XRD

XRD pattern were taken using X-ray diffraction (XRD) measurements on a Bruker-Siemens D5000 X-ray powder diffractometer equipped with a Kristalloflex 760 X-ray generator and a curved graphite monochromator using Cu Ka radiation (40 kV/30 mA). The 2θ step size was 0.03*, the integration time was 3 s per step, and the 2θ scan ranged from 10* to 90*. Diffraction patterns were compared with ICSD Database (FINDIT [41]) and analyzed by Rietveld refinement [42] using the GSAS package [43, 44].

The XRD patterns of the as-received rust and of the three iron precursors extracted after the washing treatment are shown in Fig. 5. In the as-received rust wastes, iron is present as the main phase, whereas Fe_3O_4 and iron oxyhydroxide [FeO(OH)], which is the main component of rust, were detected as secondary phases. This is not surprising since the scrapping treatment is known to take out the rusted layer together with the metallic iron underlying layers.

In the R1 washed rust both iron and Fe_3O_4 were detected more or less in the same amount, whereas iron oxyhydroxide seems to have been washed away. R2 is mainly composed by iron oxides and traces of metallic iron. The very well washed rust, R3, contains more Fe° than Fe_3O_4. From these

results, it is deduced that the suspension produced during the washing treatment is mainly composed by Fe_3O_4.

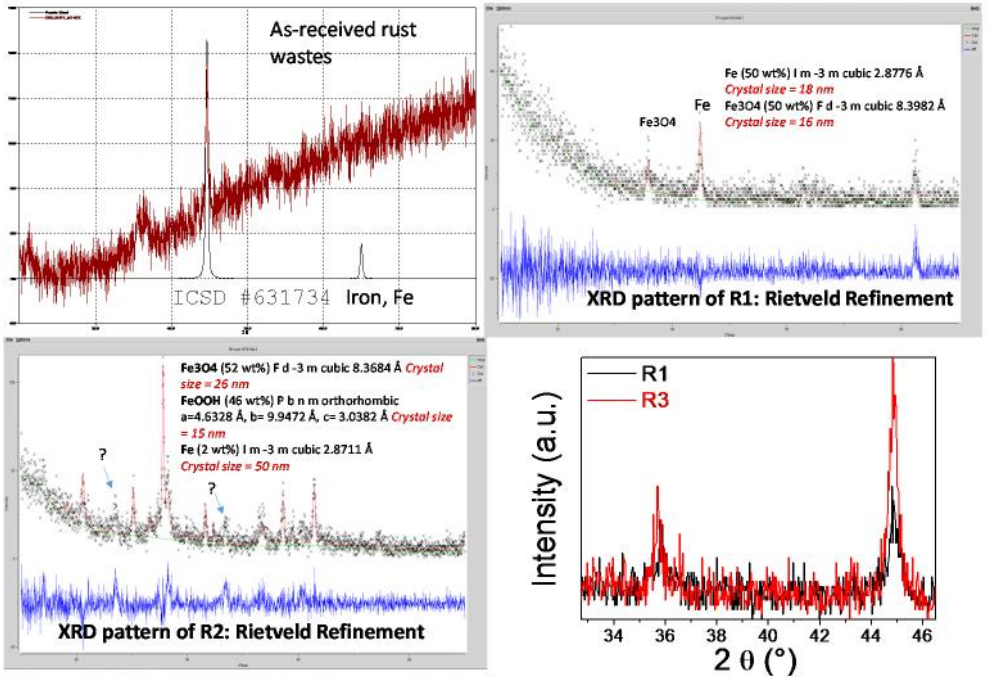

Fig 5. : X-ray diffraction patterns of the as-received rust and of the three iron precursors extracted after the washing treatment. Rietveld refinement of R1 and R2 is also shown.

FTIR

FT-IR results in Fig. 6 showed that hydrated Fe_2O_3 compounds are the main constituents of the rust wastes in agreement with the literature [3].The absence of any signal relative to metallic iron indicates that height of the rust layer cannot be higher than the detection limit of this technique. In facts that this technique allows to characterize only few micrometers of the surface, whereas XRD is a bulk characterization technique.

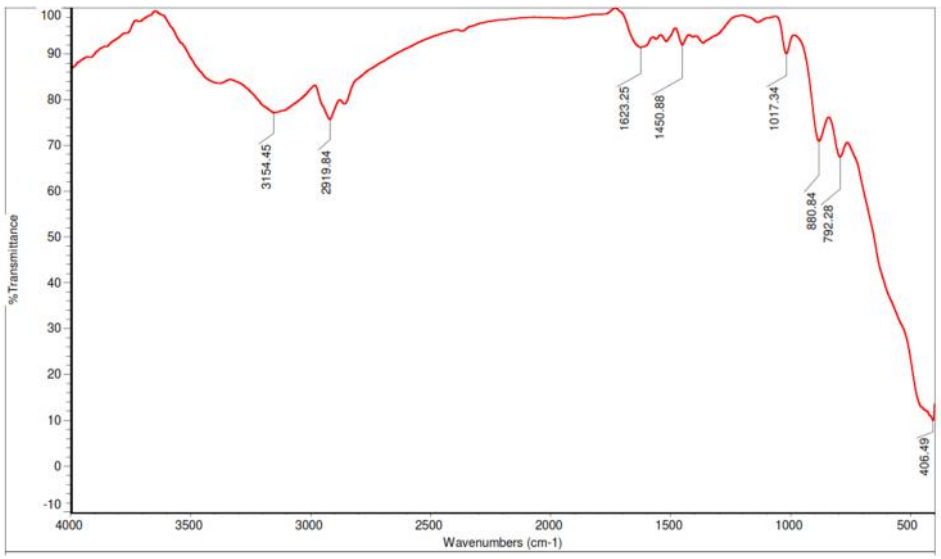

Fig 6. : FT-IR spectra of the as-received rust wastes

XPS

The experimental conditions used for the XPS measurements and analysis are analogous to those described in other papers [30].

The as-received rust and the extracted iron precursors were analyzed by XPS. The rust starting material showed a neat survey spectrum without any contaminant. After the washing treatment, no visible changes in the Fe 2p peak occurred as showed in Fig 7. The position (711 eV) and the shape showed the prevalence of FeOOH. The oxygen mainly showed two components; a low energy component at ca. 530-531eV due to lattice O^{2-} and one at 532eV attributed to surface OH^-. As evidenced by the picture, the OH^- component decreased upon washing treatment, indicating that decrease of Fe_2O_3 occurred at the surface.

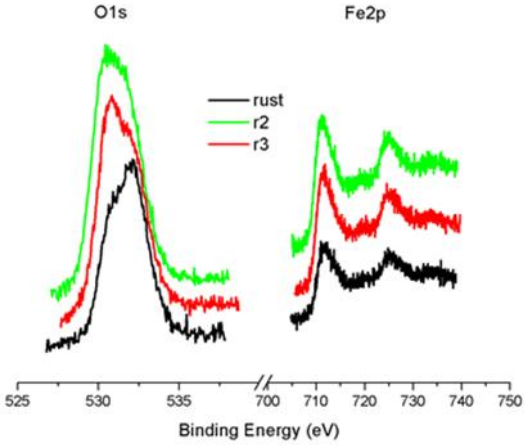

Fig 7. XPS O1s and Fe2p spectra of the as-received rust wastes and of the derived iron precursors (R1, R2, R3).

6. SYNTHESIS OF IRON-BASED COMPOUNDS

Materials used

The chemicals used were: $La(NO_3)_3.6H_2O$ (Aldrich (99.999%),Citric acid anhydrous (Alfa-Aesar 99.5+%), NH_4NO_3 (Sigma-Aldrich 99.5%) and $Fe(NO_3)_3.9H_2O$ (Alfa Aesar Puratronic 99.999%, used for the reference sample).

Synthesis procedure

Lanthanum Nitrate, citric acid, ammonium nitrate and selected amounts of rust-derived iron precursors (R1 or R2) were weighted in the required proportions and dissolved in 300 ml of distilled water. The pH was regulated at 6 with 7 ml ammonia solution. Finally, the beaker was kept on the hot plate with the vertex at 80°C and the solution was allowed to evaporate with mechanical stirring until gel formation. It was not possible to use the magnetic stirrer, since the rust-derived precursors were magnetic (see § 4) and it would attach to the magnetic needle.

After gel formation, vertex and stirrer were removed and the combustion was initiated by increasing the temperature of the hot plate to its maximum value. After combustion the as-burned powder was obtained and it was called RX (X=4-9)_NC. The as-burned powder was then kept in the furnace in an alumina crucible for calcination at 700 °C for 5 hours to get the final $LaFeO_3$.

Three samples have been prepared using R1 as a source of iron (R4_700, R5_700 and R9_700), two samples were prepared by using R2 as a source of iron (R6_700 and R8_700), and one reference sample was prepared by using $Fe(NO_3)_3.9H_2O$. Each batch produced corresponded to about 2g of $LaFeO_3$. In Fig. 8 a scheme of the synthesis procedure used is illustrated.

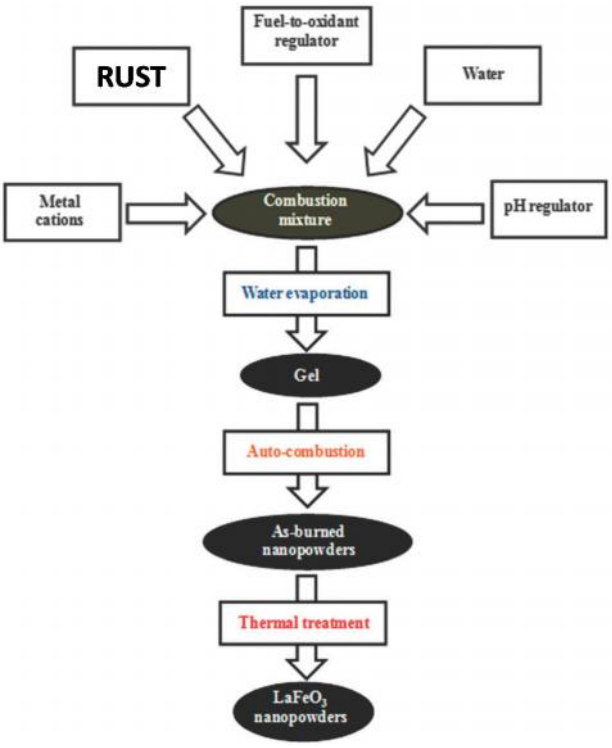

Fig 8: Flowchart with the solution combustion-based procedure used for the samples preparation and pictures showing selected steps of the synthesis

The combustion process was not very intense and it was necessary to move the combustion mass by mechanical stirring in order to extend the combustion process to the entire combustion mass. This is probably ascribed to the presence of insoluble components like iron and iron oxides, whose interaction with other components is somewhat retarded. In Fig. 9, the Temperature/Time profile of a selected sample (R5) is reported in comparison with the one registered for the reference sample.

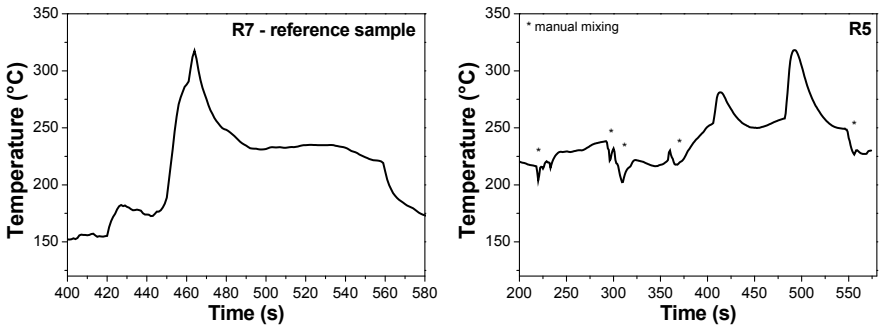

Fig 9. Temperature/ time profiles of reference sample (R7) and one selected sample (R5), registered during the combustion process.

The other samples have analogous behavior. Although the maximum temperature is still about 300°C, the combustion process of the rust derived sample is not a massive process and it is often interrupted by manual mixing (Fig. 9).

7. CHARACTERIZATION OF IRON-BASED COMPOUNDS

XRD

The perovskite-type structure was already formed in all the as-burned powders and no metallic iron was left unreacted (Fig. 10), although some segregated Fe_2O_3 was found in all the samples except in R4_NC and in the reference sample (R7_NC).

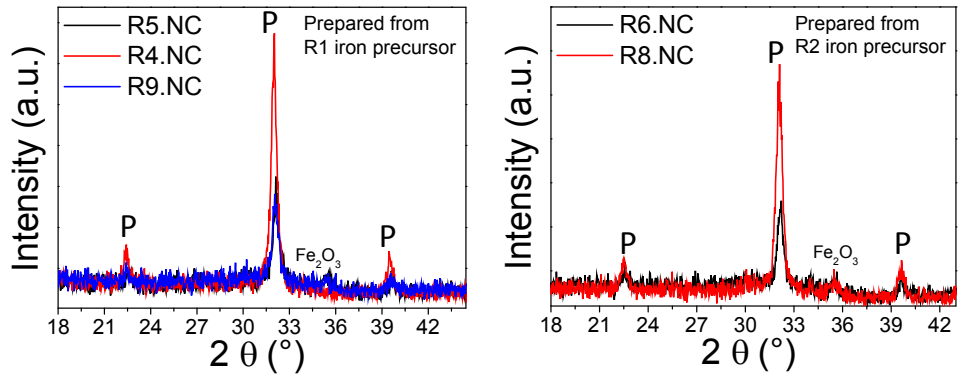

Fig 10. Enlargement of the X-ray diffraction patterns of as-burned RX_NC powders prepared from R1 iron precursor (left) and from R2 iron precursor (right).

After calcination at 700°C, the perovskite structure is fully formed (Fig 11).

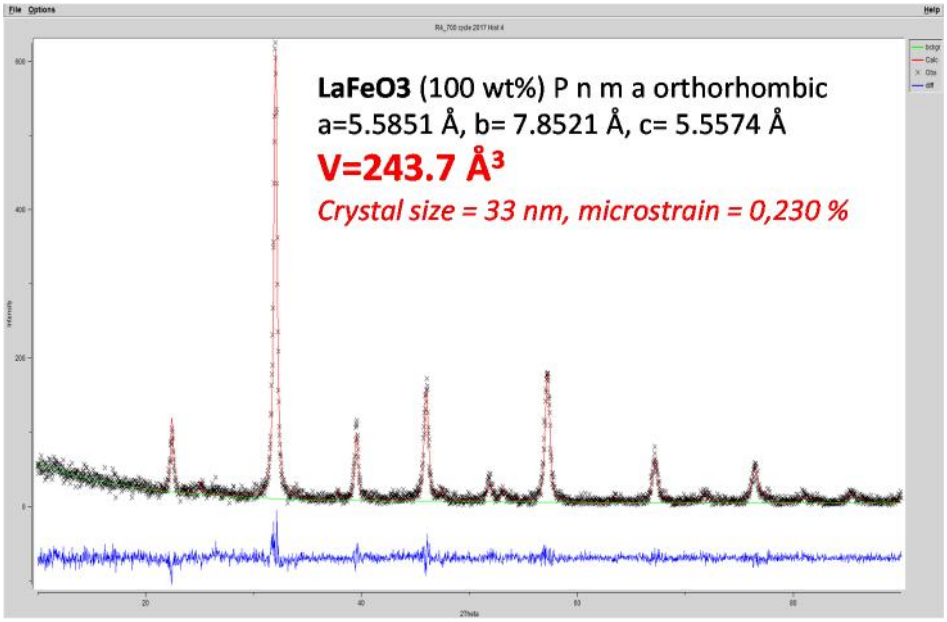

Fig 11. XRD pattern of R4_700 and Rietveld refinement.

Nevertheless, even after calcination, there is still some Fe_2O_3 segregated in the XRD patterns of all the samples (Fig. 12), except in R4_700 and in the reference R7_700.

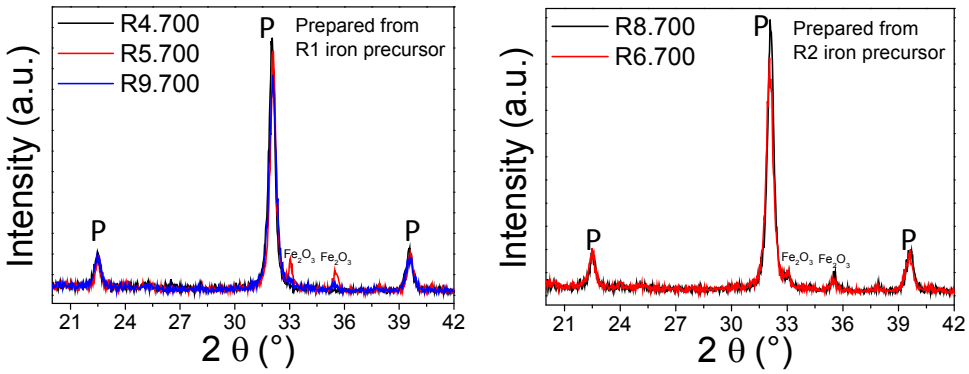

Fig 12. Enlargement of the X-ray diffraction patterns of calcined RX_700 powders prepared from R1 iron precursor (left) and from R2 iron precursor (right).

In Table 1, phase composition and structural parameters of all the calcined samples are reported. In the same table, the type/amount of iron precursor used is specified.

Sample	Type of iron precursor	gr of iron precursor	Phase Composition (wt.%)	Cell Volume (Å^3)	Crystal size of $LaFeO_3$ (nm)	Microstrain (ε%)
R7_700	***$Fe(NO_3)_3 \cdot 9H_2O$***	**3,328**	**$LaFeO_3$ (100 wt%)**	**243,2**	**49**	**0,079**
R4_700	*R1*	0,460	$LaFeO_3$ (100 wt%)	243,7	33	0,230
R9_700	*R1*	0,802	$LaFeO_3$ (92 wt%) Fe_2O_3 (8 wt%)	242,9	45	0,188
R5_700	*R1*	1,184	$LaFeO_3$ (77 wt%) Fe_2O_3 (23 wt%)	243,1	31	0,135
R8_700	*R2*	1,101	$LaFeO_3$ (85 wt%) Fe_2O_3 (15 wt%)	243,2	33	0,270
R6_700	*R2*	1,338	$LaFeO_3$ (87 wt%) Fe_2O_3 (13 wt%)	243,1	28	0,222

Table1. La/Fe ration, O1s, Fe2p and La3d binding energies of the reference and three other selected samples

The percentage of segregated Fe_2O_3 increases with amount of iron precursor for rust derived sample. All the cell parameters are comparable to the reference sample, except for R4_700, which has a slightly larger cell volume. Crystal size of the perovskite phase is about 30 nm for all the samples, except R9_700 and the reference. Microstrain is slightly higher for the rust derived samples.

TPR

The TPR results are displayed in the following figures. The TPR profile for R9 (red curve) shows two different regions between 380-400 °C and 670-700 °C.

The TPR profile for R7 (Reference, blue curve) indicates negligible reduction as can be seen in the following curve whereas the TPR profile for R4 showed two peaks at 300 -320 °C and 530-550 °C . According to literature, the peak at lower temperatures represents the reduction of the absorbed oxygen on the catalyst surface and the second one at higher temperature is correlated to the reduction of the lattice oxygen in the bulk [1]. The TPR profile of R4, R7 (Reference) and R9 indicates that there are some evident differences in the reducibility of these powders at the catalyst surface.

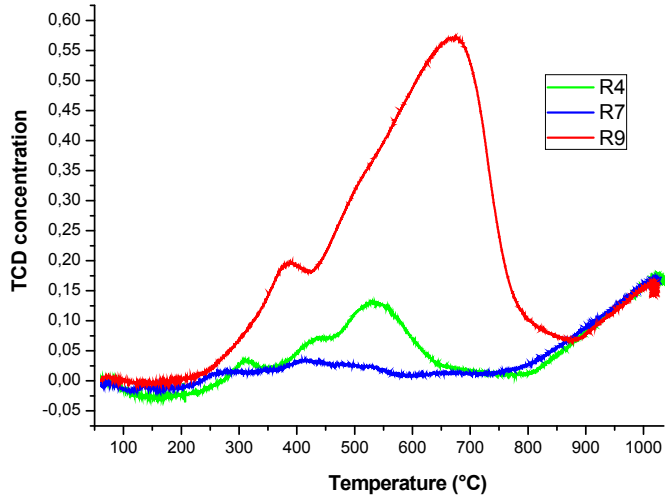

Fig 13. TPR curves of the R7_700 reference sample and two other selected samples prepared from R1

According to the theoretical calculations, assuming that all the starting powder is $LaFeO_3$ and that all the Fe is in its trivalent state, it was calculated that the reduction process was not completed even at 1000°C.

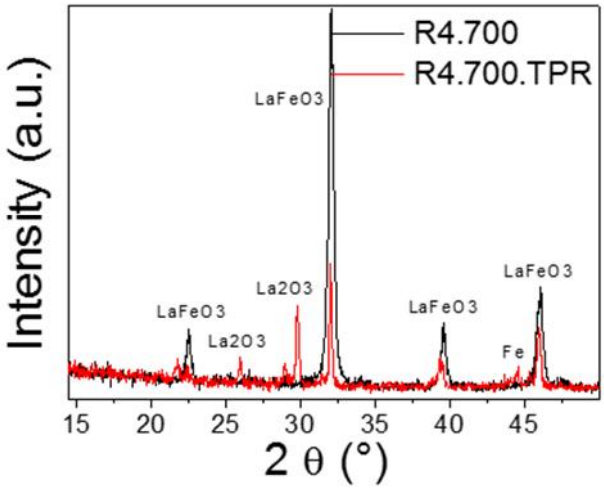

Fig 14. XRD patterns of R4_700 before and after TPR experiments

Fig 14 shows XRD patterns of R4_700 before and after TPR: the perovskite is more than half destroyed, but not completely, in agreement with the calculations. Reduction products are Fe and La_2O_3.

XPS

Fig 15. Comparison between XPS O1s and Fe2p spectra of the R6_700 sample and of the R3 iron precursor.

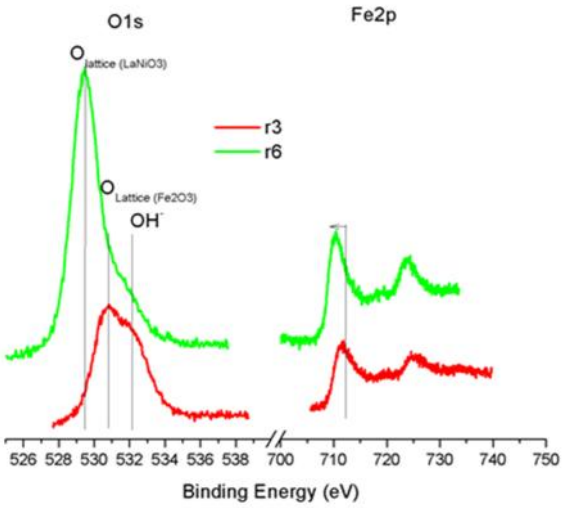

By comparing the O1s and Fe2p spectra of the calcined products (all of them very similar in position), we confirm the incorporation of iron in the perovskites structure, as evidenced by the downshift of Fe2p and O1s peaks. The Lanthanum position is also typical of perovskites materials.

Sample	La/Fe	O1s	Fe2p	La3d
R4_700	2.2	529.0 (57%) 531.5 (40%) 533.5 (3%)	709.8	833.6
R5_700	0.7	529.3 (48%) 530.4 (46%) 532.3 (6%)	710.4	833.8
R6_700	0.7	529.4 (79%) 531.4(13%) 532.2 (8%)	710.0	833.5
R7_700	1.9	529.4 (65%) 531.7 (26%) 533.0 (9%)	710.0	833.8

Table 2. La/Fe ration, O1s, Fe2p and La3d binding energies of the reference and three other selected samples

The ratio between La and Fe changes in the different preparations (Table 2) and this is in accord with XRD characterizations. Oxygen peaks show component due to perovskites lattice (*ca.* 529 eV), to more surface oxygen generate by OH terminal groups (*ca.* 531 eV) and to absorbed water (ca. 533 eV).

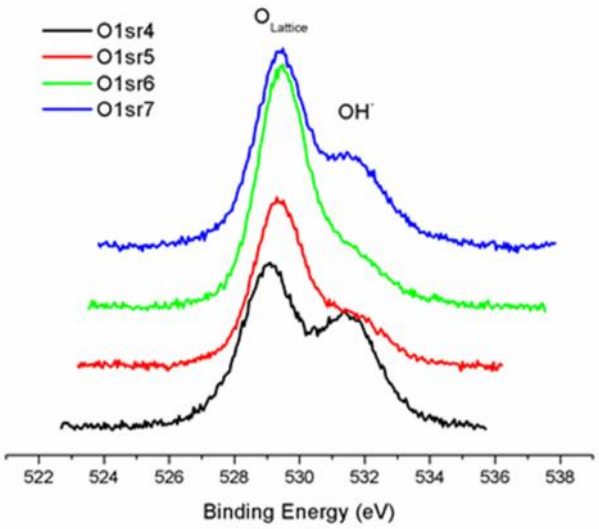

Fig 17. XPS O1s spectra of the reference and of three selected samples (R4, R5, R6)

The variation of these two components may be indicative of the formation of segregated Fe_2O_3 (O1s at *ca.* 530 eV), or of different oxygen vacancies (in agreement with TPR results).

8. APPLICATION OF IRON-BASED COMPOUNDS

Propylene Oxidation test

Activity tests were carried out in a continuous flow using a U-shaped quartz reactor operated at atmospheric pressure. The reactor temperature was measured by a thermocouple placed co-axially inside the reactor. The feeding was a gas mixture having 2500 ppm of propylene and 15% O_2 (balance He). An amount of 50 mg of sample was used for each run corresponding to a WHSV (weight hourly space velocity) of 60000 $ml \cdot gr^{-1}h^{-1}$. The catalyst bed was supported by glass wool. The activity tests were performed between I00-500°C with steps of 25 *C and waiting 30 minutes for each step in order to get steady state conditions.

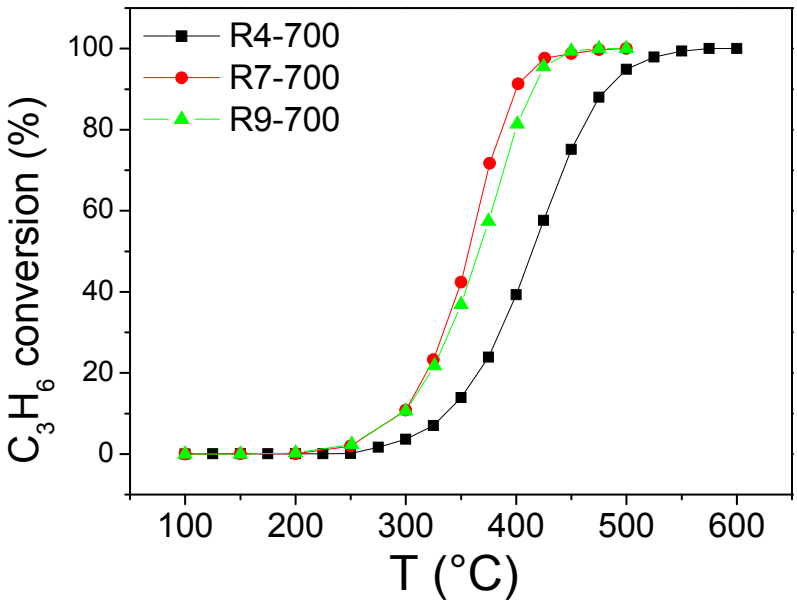

Fig. 18 : Comparison of C_3H_6 conversion between the reference sample (R7_700) and two rust waste-derived samples (R9-700 and R4_700).

The feed and the effluent gases were analyzed using UV-IR ABB Analyzers to detect CO and CO_2 and a paramagnetic analyzer for O_2. The propylene conversion was evaluated based on the detected CO and CO_2.

In general, conversion increased with increase in the temperature for all the three samples i.e. R4-700, R7-700 and R9-700. Three samples have been tested and the reactivity pattern for $LaFeO_3$ catalysts was found to be in the following order: R7-700 ~ R9-700 > R4-700. An almost comparable activity to the reference was obtained for the rust-derived sample R9_700, indicating that the proposed synthetic approach has succeeded.

9. CONCLUDING REMARKS

For the first time an iron perovskite has been successfully prepared by solution combustion based methodologies from rust wastes-derived iron precursors, demonstrating that the replacement of commercial iron precursors is possible.

The obtained powders contained some segregated Fe_2O_3 phase, depending on the type/amount of the iron precursor used for the synthesis. This secondary phase affects the surface and the redox properties of the powders, although it does not seem to hinder the propylene oxidation activity to a great extent.

The detailed characterization of the iron precursors and the obtained powders evidenced an important role of the iron precursor in the properties of the final powders.

FUTURE DEVELOPMENTS

The proposed approach can be easily extended to the preparation of doped $LaFeO_3$ and other iron-containing compounds, enabling the sustainable production of a variety of functional materials.

10. REFERENCES

[1] $La_{1-x}Sr_xCo_{1-y}Fe_yO_{3-\delta}$ perovskites: Preparation, characterization and solar photocatalytic activity, E. García-López, G. Marcì, F. Puleo, V. La Parola, L.F. Liotta, *Applied Catalysis B: Environmental* 178 (2015) 218–225.

[2] B-Site Metal (Pd, Pt, Ag, Cu, Zn, Ni) Promoted $La_{1-x}Sr_xCo_{1-y}Fe_yO_{3-\delta}$ Perovskite Oxides as Cathodes for IT-SOFCs, Shaoli Guo, Hongjing Wu , Fabrizio Puleo and Leonarda F. Liotta, *Catalysts* 2015, 5, 366-391; $La_{0.6}Sr_{0.4}FeO_{3-\delta}$ and $La_{0.6}Sr_{0.4}Co_{0.2}Fe_{0.8}O_{3-\delta}$ Perovskite Materials for H_2O_2 and Glucose Electrochemical Sensors, L. F. Liotta F. Puleo, V. La Parola, S. G. Leonardi, N. Donato, D. Aloisio and G. Neri, *Electroanalysis* 2015, 27, 684 – 692.

[3] R. Balasubramaniam, A. V. Ramesh Kumar, P. Dillmann, "Characterization of rust on ancient Indian iron", CURRENT SCIENCE, VOL. 85, NO. 11, 10 DECEMBER 2003.

[4] https://commons.wikimedia.org/wiki/File:Corroding_machinery_at_old_White_Island_sulphur_mine.JPG

[5] UNION INTERNATION ASSOCIATIONS – WORLD PROBLEMS http://www.uia.be/sites/uia.be/db/db/x.php?dbcode=pr&go=e&id=11519450)

[6] Zainab Z. Ismail, Enas A. AL-Hashmi, "*Reuse of waste iron as a partial replacement of sand in concrete*", Waste Management 28 (2008) 2048–2053.

[7] Dattakumar Mhamane, Kwang Chul Roh, Hyun-Kyung Kim, Madhavi Srinivasan, Vanchiappan Aravindan, Kwang-Bum Kim, "*Rusted iron wire waste into high performance anode (α-Fe2O3) for Li-ion batteries: an efficient waste management approach*", Green Chem., 2016, 18, 1395–1404.

[8] John Adeola Adegoke, I. Adegoke Halimat, "*Absorption Studies of Arsenic Using Maghemite Crystals Synthesized from Iron Waste Extracted from Ogun State Iron Mill Dumpsite*", American Journal of Analytical Chemistry, 2016, 7, 294-298.

[9] Jin Wu, Luming Ma, Yunlu Chen, Yunqin Cheng, Yan Liu, Xiaosong Zha, "*Catalytic ozonation of organic pollutants from bio-treated dyeing and finishing wastewater using recycled waste iron shavings as a catalyst: Removal and pathways*", Water Research 92 (2016) 140-148.

[10] Sahar Naim, Antoine Ghauch, "*Ranitidine abatement in chemically activated persulfate systems: Assessment of industrial iron waste for sustainable applications*", Chemical Engineering Journal, 288 (2016) 276–288.

[11] Xiang Li, Chuankai Wang, Yu Zeng, Panyu Li, Tonghui Xie, Yongkui Zhang, "*Bacteria-assisted preparation of nano α-Fe_2O_3 red pigment powders from waste ferrous sulfate*"

[12] L.Yu. Novoselova, "*Hematite nanopowder obtained from waste: Iron-removal sludge*", Powder Technology 287 (2016) 364–372.

[13] Bo Liu, Shen-gen Zhang, De-an Pan, Chein-chi Chang, "*Synthesis and characterization of micaceous iron oxide pigment from oily cold rolling mill sludge*" Procedia Environmental Sciences 31 (2016) 653 – 661.

[14] Robert C. Pullar, Manfredi Saeli, Rui M. Novais,, Joao S. Amaral, Joao A. Labrincha, "*Valorisation of industrial iron oxide waste to produce magnetic barium hexaferrite*", ChemistrySelect 2016, 4, 819 –825.

[15] Yanping Wang, Junwu Zhu, Lili Zhang, Xujie Yang, Lude Lu, Xin Wang, "*Preparation and characterization of perovskite $LaFeO_3$ nanocrystals*", Materials Letters, 60 (2006) 1767–1770.

[16] K.C. Patil, S.T. Aruna, T. Mimani *Combustion synthesis: an update* Curr. Opin. Solid State Mater. Sci., 6 (2002), pp. 507–512.

[17] A. Varma, A. S. Mukasyan, A. S. Rogachev, K. V. Manukyan, "*Solution Combustion Synthesis of Nanoscale Materials*," Chem. Rev., vol. 116, no. 23, pp. 14493-14586, September 2016.

[18] F. Deganello, G. Marcì, G. Deganello, "*Citrate-nitrate auto-combustion synthesis of perovskite-type nanopowders: a systematic approach*," J. European Ceram. Soc., vol. 29, no. 3, pp. 439-450, February 2009.

[19] S.R. Jain, K.C. Adiga, V.R. Pai Verneker *A new approach to thermochemical calculations of condensed fuel–oxidizer mixtures* Combust. Flame, 40 (1981), pp. 71–79.

[20] C.-C. Hwang, T.-H. Huang, J.-S. Tsai, C.-S. Lin, C.-H. Peng *Combustion synthesis of nanocrystalline ceria (CeO2) powders by a dry route*, Mater. Sci. Eng. B, 132 (2006), pp. 229–238

[21] A.S. Mukasyan, P. Epstein, P. Dinka Solution combustion synthesis of nanomaterials, Proc. Combust. Inst., 31 (2007), pp. 1789–1795.

[22] A.K. Tyagi, S.V. Chavan, R.D. Purohit A visit to the fascinating world of nano-ceramics powders via solution-combustion Ind. J. Pure Appl. Phys., 44 (2006), pp. 113–118.

[23] W. Chen, F. Li, J. Yu A facile and novel route to high surface area ceria-based nanopowders by salt-assisted solution combustion synthesis, Mater. Lett., 60 (2006), pp. 57–62.

[24] V. Bedekar, V. Grover, S. Nair, R.D. Purohit, A.K. Tyagi Nanocrystalline electroceramics by combustion method, Synth. React. Inorg. Met.-Org. Nano-Met. Chem., 37 (2007), pp. 321–326.

[25] Q. Xu, D.-P. Huang, W. Chen, J.-H. Lee, H. Wang, R.-Z. Yuan Citrate method synthesis, characterization and mixed electronic–ionic conduction properties of La0.6Sr0.4Fe0.2Co0.8O3 perovskite-type complex oxides, Scr. Mater., 50 (2004), pp. 165–170.

[26] A. Majid, J. Tunney, S. Argue, D. Wang, M. Post, J. Margeson Preparation of SrFeO2.85 perovskite using a citric acid assisted Pechini-type method, J. Alloys Compd., 398 (2005), pp. 48–54.

[27] P. Palmisano, N. Russo, P. Fino, D. Fino, C. Badini High catalytic activity of SCS-synthesized ceria towards diesel soot combustion, Appl. Catal. B: Environ., 69 (2006), pp. 85–92.

[28] M.D. Carvalho, F.M.A. Costa, I. da Silva Pereira, A. Wattiaux, J.M. Bassat, J.C. Grenier, et al., New preparation method of Lan+1NinO3n+1-δ (n = 2, 3), J. Mater. Chem., 7 (1997), pp. 2107–2111.

[29] F. Deganello, M.L. Tummino, C. Calabrese, M.L. Testa, P. Avetta, D. Fabbri, A. Bianco Prevot, E. Montoneri, G. Magnacca, "*A new, sustainable $LaFeO_3$ material prepared from biowaste-sourced soluble substances*," New J. Chem., vol. 39, no. 2, pp. 877-885, February 2015.

[30] F. Deganello, M. L. Testa, V. La Parola, A. Longo, A.Tavares, *$LaFeO_3$-based nanopowders prepared by a soft-hard templating approach: the effect of silica texture*, J. Mater. Chem. A, 2 (2014) 8438-8447.

[31] Hansu Birol, Carlos Renato Ramb, Marcela Guiotoku, Dachamir Hotza, "*Preparation of ceramic nanoparticles via cellulose-assisted glycine nitrate process: a review*", RSC Adv., 2013,3, 2873-2884.

[32] Felicity H. Taylor,John Buckeridge, C. Richard A. Catlow, "*Defects and Oxide Ion Migration in the Solid Oxide Fuel Cell Cathode Material $LaFeO_3$*", Chem. Mater. 2016, 28, 8210−8220.

[33] G. Magnacca, G. Spezzati, F. Deganello, M. L. Testa, "*A new in situ methodology for the quantification of the oxygen storage potential in perovskite-type materials*, " RSC Adv., vol. 3, no. 48, pp. 26352-26360, December 2013.

[34] Ensi Cao, Yuqing Yang, Tingting Cui, Yongjia Zhang, Wentao Hao, Li Sun, Hua Peng, Xiao Deng, "Effect of synthesis route on electrical and ethanol sensing characteristics for $LaFeO_{3-\delta}$ nanoparticles by citric sol-gel method", Applied Surface Science 393 (2017) 134–143.

[35] Peisong Tang, Mengbi Fu, Haifeng Chen , Feng Cao, "*Synthesis of Nanocrystalline $LaFeO_3$ by precipitation and its Visible-Light Photocatalytic Activity*", Materials Science Forum, 694, pp 150-154.

[36] K.T.C. Roseno, R. Brackmann, M.A. da Silva, M. Schmal, "*Investigation of $LaCoO_3$, LaFeO3 and LaCo0.5Fe0.5O3 perovskites as catalyst precursors for syngas production by partial oxidation of methane*", Int. J. Hydrogen En., 41 (2016) 18178–18192.

[37] Hisahiro Einaga, Yusaku Nasu, Manabu Oda, Hikaru Saito, "*Catalytic performances of perovskite oxides for CO oxidation under microwave irradiation*", Chem. Eng. J., 283 (2016) 97–104.

[38] Guillaume Tesquet, Jérémy Faye, Fadime Hosoglu, Anne-Sophie Mamede, Franck Dumeignil, Mickaël Capron, *"Ethanol reactivity over La 1+xFeO3+δ perovskites*", Applied Catalysis A: General 511 (2016) 141–148.

[39] J. Faye, E. Guelou J. Barrault J. M. Tatibouet, S. Valange, "*$LaFeO_3$ Perovskite as New and Performant Catalyst for the Wet Peroxide Oxidation of Organic Pollutants in Ambient Conditions*", Top Catal (2009) 52:1211–1219.

[40] Young-Gil Cho, Kyong-Hoon Choi,Yong- Rok Kim, Jin-Seung Jung,, Sung-Han Lee, "*Characterization and Catalytic Properties of Surface La-rich $LaFeO_3$ Perovskite*", Bull. Korean Chem. Soc. 2009, Vol. 30, No. 6.

[41] Findit version 1.9.7 Inorganic Crystal Structure Database (ICSD)

[42] L. B. McCusker, R. B. Von Dreele, D. E. Coxd, D. Louer and P. Scardi, J. Appl. Crystallogr., 1999, 32, 36.

[43] A.C. Larson and R.B. Von Dreele, "General Structure Analysis System (GSAS)", Los Alamos National Laboratory Report LAUR 86-748 (2000)

[44] B. H. Toby, *EXPGUI*, a graphical user interface for *GSAS*, *J. Appl. Cryst.* **34**, 210-213 (2001).